ice | science

ICE SCIENCE – Keywords
Stratlingite; Structure; Microstructure; Synchrotron X-ray powder diffraction; Rietveld refinement; Belite calcium sulfoaluminate cements.

ice Institution of Civil Engineers publishing

Structure of stratlingite and effect of hydration methodology on microstructure

***Isabel Santacruz,** Dr.
Departamento de Química Inorgánica, Cristalografía y Mineralogía, Universidad de Málaga, 29071-Málaga, Spain
Tel.: +34952131992; fax: +34952131870. E-mail address: isantacruz@uma.es
Ángeles G. De la Torre, Dr.
Departamento de Química Inorgánica, Cristalografía y Mineralogía, Universidad de Málaga, 29071-Málaga, Spain
Gema Álvarez-Pinazo, PhD Student.
Departamento de Química Inorgánica, Cristalografía y Mineralogía, Universidad de Málaga, 29071-Málaga, Spain
Aurelio Cabeza, Dr.
Departamento de Química Inorgánica, Cristalografía y Mineralogía, Universidad de Málaga, 29071-Málaga, Spain
Ana Cuesta, PhD Student.
Departamento de Química Inorgánica, Cristalografía y Mineralogía, Universidad de Málaga, 29071-Málaga, Spain
Jesús Sanz, Dr.
Instituto de Ciencia de Materiales de Madrid (ICMM), Consejo Superior de Investigaciones Científicas (CSIC), Cantoblanco, 28049-Madrid, Spain.
Miguel A. G. Aranda. Professor.
Departamento de Química Inorgánica, Cristalografía y Mineralogía, Universidad de Málaga, 29071-Málaga, Spain
CELLS-Alba Synchrotron, Carretera BP 1413, Km. 3.3, E-08290 Cerdanyola, Barcelona, Spain

Abstract

Stratlingite, $Ca_4Al_2(OH)_{12}[AlSi(OH)_8]_2 \cdot 2H_2O$, is an AFm phase which appears as hydration product of aluminum-rich cements. These binders may be calcium aluminate cements, calcium sulfoaluminate cements and also Belite Calcium Sulfo-Aluminate (BCSA) cements. The structure of stratlingite is known from single crystal studies of tiny minerals but their bulk formation, crystal structure and microstructure of powders is poorly understood. Here, we report the synthesis of stratlingite and a complete structural and microstructural characterization by synchrotron X-ray powder diffraction, nuclear magnetic resonance, scanning electron microscopy and thermal analyses. The structural and microstructural models have important implications for a correct quantitative phase analysis of stratlingite in cement pastes (for instance, in pastes of BCSA cements). The microstructure of stratlingite formed in cement pastes is highly dependent on the hydration conditions. In BCSA pastes, the (003) line position of stratlingite appears slightly shifted towards higher diffracting angles (lower inter-layered distance) after stopping hydration compared to that of a similar phase present in a paste analyzed without stopping hydration. This is related to dehydration and disorder. This shift and peak broadening is even larger when the paste has suffered partial dehydration during curing (apart from stopping hydration). A microstructural study is reported.

1. Introduction

Ordinary Portland Cement (OPC) production accounts for 6% of anthropogenic carbon dioxide emissions and for 4% of total global warming (McCaffrey, 2002; Gartner, 2004). The interest in eco-cements with new formulations arises from their potential to release up to 40% less CO_2 than OPC in their manufacture, depending on their composition. In the last few years, Belite Calcium Sulfo-Aluminate (BCSA) cements, also known as sulfobelite cements, are being developed as OPC substitutes (Gartner, 2006; Cuberos et al., 2010; Morin et al., 2011). Although they have been proposed as a sustainable alternative to OPC, some technological challenges (Álvarez-Pinazo et al., 2013), such as relatively low mechanical strengths and durability, should be improved. The understanding of the hydration processes (Winnefeld and Lothenbach, 2010; Klaus et al., 2013; Le Saoût et al., 2013) should lead to an improved design of the clinker

composition (activation) and better performances after setting and hardening.

During the hydration process of calcium sulfoaluminate cements (CSA) and BCSA cements (Sahu et al., 1991; Marchi et al., 2011), three main issues take place: i) dissolution of crystalline anhydrous phases, ii) appearance of new phases (Aranda et al., 2012) such as crystalline stratlingite ($Ca_4Al_2(OH)_{12}[AlSi(OH)_8]_2 \cdot 2H_2O$) and amorphous gels; iii) consumption of free water. In order to properly study these processes, there is an increasing interest in the synthesis and advanced characterization (Balonis and Glaser, 2009) of single phases that are involved in the hydration of cements, such as ye'elimite (Cuesta et al., 2013), belite (Cuesta et al., 2012; Cuesta et al., 2014), alite (De la Torre et al., 2002), katoite (Dilnesa et al., 2014), stratlingite (Kwan et al., 1995), and so on. The formation of these new crystalline phases in the cement pastes can be determined and quantified through X-Ray Powder Diffraction (XRPD) jointly with the Rietveld methodology. Hence, the knowledge of the structure (and microstructure) of these individual phases makes possible the control of the hydration of the cement pastes and then, the design of cement/mortars with improved properties/performances.

In this context, it is important the full characterization of stratlingite as this is an AFm-type phase which appears as hydration product of aluminum-rich cements. These binders may be calcium aluminate cements, CSA and BCSA cements. Stratlingite is not formed by direct hydration of OPC, but it has been reported in the hydration of Portland binders with Al_2O_3-rich additions (for instance, fly ashes). Stratlingite is a mineral found as a metamorphosed limestone inclusion within the basaltic lava flow at Bellerberg, Mayern/Eifel (Hentschel and Kuzel, 1976; Fleischer and Jambor, 1977) and in a marly inclusion in a phonolitic lava (Campomorto, Italy, near Montalto di Castro) (Passaglia and Turconi, 1982).

A few methods have been reported for the preparation of stratlingite, including: i) reaction between calcium hydroxide and metakaolin in suspension (Taylor, 1997); depending on the composition and conditions, similar reactions of natural pozzolans can yield, besides calcium silicate hydrate gel, stratlingite or hydrogarnet. Stratlingite was first synthesized by this method. ii) From a stoichiometric mixture of oxides (SiO_2, Al_2O_3 and CaO) with excess water at room temperature (RT) for 1.5-2 years (Kwan et al., 1995); this method produced poorly crystallized stratlingite. In an attempt to increase its crystallinity, the same authors treated hydrothermally the resulting suspension, 150°C overnight. iii) Stoichiometric mixture of calcium aluminate cement, CaO and metakaolinite for 3 days in the presence of alkali (Kwan et al., 1995). iv) Slow hydration of calcium aluminum silicate glasses in saturated solutions of $Ca(OH)_2$ at 20°C for 120 days (Kuzel, 1976). v) Stoichiometric mixture of CaO, $Na_2Si_2O_5 \cdot 2H_2O$ and $NaAlO_2$ in water, which was stirred for 4 weeks at RT prior to filtration (Balonis and Glasser, 2009; Matschei et al., 2007b). The best result seems to be obtained by this last route. Some properties of these stratlingite powders (cell dimensions, space group, density, etc.) are described elsewhere (Balonis and Glasser, 2009).

Stratlingite, like any AFm-type phase has a layer structure with the following general formula $[Ca_2Al(OH)_6]X \cdot yH_2O$. For stratlingite, X is the $[SiAlO_2(OH)_4]^-$ anion which forms a double tetrahedral layer containing ~50% vacancies. Moreover, iron-bearing stratlingite may also be formed by partial substitution of aluminum in the octahedral layer (Wang, 2010). Rinaldi et al.(1990) described the crystal structure of stratlingite (mineral fragments from Mayern and Montalto di Castro) as: a) a principal octahedral or brucite-type layer, $[Ca_2Al(OH)_6 \cdot 2H_2O]^+$ with a full occupancy, and b) a double tetrahedral layer, $[(T,\square)_4(OH,O)_8 \cdot 0.25H_2O]^-$, with a 45% of vacancies. The octahedral layer has an overall positive charge, and the double tetrahedral layer negative. They proposed a Si/Al atomic ratio of 1, where Si-Al order was not detected. The reduced chemical formula derived from the structure refinement was $Ca_2Al(Al,Si)_{2.28}O_2(OH)_{12} \cdot 2.25H_2O$, where the unbalanced charge should be compensated with a Si/Al atomic ratio slightly different from 1 or the possible vacancy of some anionic sites. The symmetry of stratlingite is R3m. The structure analysis (Rinaldi et al., 1990) indicates that the octahedral layer shows an ordered scheme where each Al-octahedron is linked to 6 edge-sharing Ca^{VII} polyhedra (2 out 3 positions are then occupied by the seven coordinated Ca-type cation). When present, sodium ions could substitute for calcium ions in this layer. The structure also contains hydration water. Most of the water is located in the aluminum octahedral layer (in the seventh vertex, Ow2) projecting towards the centre of the 6-membered rings of the double tetrahedral layers. These water molecules form hydrogen bonds between the neighboring octahedral and tetrahedral layers and tend to hold the modules together. One additional water molecule site (Ow1, with partial occupancy) was located at the centre of the 6-rings of the double tetrahedral-layers. In addition, the double tetrahedral layers shows an unusual (energetically unstable) T-O-T angle (where T means tetrahedral) of 180°, which may be favored by the large proportion of vacancies (Rinaldi et al., 1990) or being the result of long range averaging but locally bent.

These conclusions were corroborated by Kwan et al. (1995) through the characterization of synthesized-stratlingite powder (from oxides) by some techniques, such as Nuclear Magnetic Resonance (NMR). These authors confirmed that the aluminum atoms are both tetrahedral and octahedral, and the silicon atoms exist predominantly as Q_2, $Q_2(1Al)$ and $Q_2(2Al)$ species. The

presence of alkali affects the structure of stratlingite in subtle ways, significantly reducing the Al^{IV}/Al^{VI} ratio. Similar to Rinaldi (1990), Kwan et al. (1995) confirmed that the aluminum substitution in the six-membered rings present in stratlingite (synthesized from oxides) seem to be random and equally divided among Q_2, $Q_2(1Al)$, and $Q_2(2Al)$ sites, all bands having approximately the same area. However, this sample also exhibits evidence for a possible $Q_3(2Al)$ component which may have OH-ions associated with it. This suggests that the 45% vacancies of the six-membered rings in the double tetrahedral layers are breaking up the network structure. This reduces the network to a series of complex silicate rings structures which occasionally bond to each other. A Q_3 silicate anion occurs when two of the rings share a silicon atom by cross linking. The data suggested that the relative ratio of Q_2/Q_3 should be much higher than 1.

Additionally, it is important to understand the performances for specific applications, such as nuclear waste containments and long-lived infrastructure developments. In this sense, the response under high pressures is important. Moon et al. (2011) studied the effects of pressure on the structure of synthesized-stratlingite (Matschei et al., 2007a) through Synchrotron X-Ray Powder Diffraction (SXRPD). The sample showed a sudden volume contraction around 1.5 GPa, where the estimated volume was 1035.67 $Å^3$, and transformed irreversibly to an amorphous phase at 3.4 GPa. Per formula unit of stratlingite, the interlayer/tetrahedral unit, $[AlSi(OH)_8 \cdot H_2O]^-$, contains only one molecule of water. Considering the hypothesis of pressure-induced dehydration, the stiffness of the crystal should increase once water molecules move out from the calcium aluminosilicate framework. This phenomenon was confirmed by these authors where an increase in stiffness is observed for pressures greater than 1.5 GPa. The slight rearrangements of structural elements, even if several weak interlayer water bonds are broken, are not enough to destroy the crystal framework of the sample, which transforms from stratlingite to "metastratlingite".

There is a double objective in this work. Firstly, to synthesize stratlingite, perform a complete structural and microstructural characterization including SXRPD, NMR, scanning electron microscopy (SEM) and thermal analyses; secondly to study the implications of our revised structure and microstructure on the quantitative phase analysis of BCSA eco-cement pastes prepared under different hydration conditions at the same aging time.

2. Materials and methods

2.1. Materials

2.1.1. Preparation of stratlingite.

Stratlingite was synthesized following a similar methodology to that reported in references (Balonis and Glasser, 2009; Matschei et al., 2007b). Stoichiometric mixtures of $Na_2SiO_3 \cdot 5H_2O$ (Aldrich), $NaAlO_2$ (Sigma-Aldrich) and CaO (from $CaCO_3$, Alfa Aesar) were added into double boiled distilled water at 20ºC. The water/solid ratio was 10, and the raw mixture was prepared with the amounts of starting materials needed for obtaining 5 g of stratlingite. The suspension was stirred for 8 weeks at 20ºC. Then, the sample was pressure-filtered in a dry chamber with N_2, and washed by flushing with double boiled distilled water (twice) to eliminate any remaining sodium (Matschei et al., 2007b), and flushed with acetone (once) for drying. Finally, the resulting powder was dried for 2 days in a stove at 30ºC.

2.1.2. Preparation of Belite Calcium SulfoAluminate (BCSA) cement pastes.

Laboratory BCSA clinker (Álvarez-Pinazo et al., 2012) and pastes (Álvarez-Pinazo et al., 2013) were prepared as previously reported. The as-prepared BCSA paste was gathered in 2 groups and treated as follow: a) transferred into a methacrylate sample holder covered with plastic wrap and statically stored in a humidity chamber at 99% relative humidity (RH); b) cast in a hermetically closed polytetrafluoroethylene (PTFE) cylinder shape mold rotated at 15 rpm for 24 hours. After that time, this sample was kept in deionized water. Both groups of samples were kept at 20 ± 1ºC for a total of 7 days.

Prior to Laboratory X-Ray Powder Diffraction (LXRPD) characterization, pastes were ground to fine powder in an agate mortar. The hydration of the pastes was stopped prior LXRPD characterization. The experimental procedure to stop the hydration consists on filtration with acetone and ether as it is reported elsewhere (García-Mate et al., 2013). Furthermore, the ground powder, prepared by b) procedure, was characterized with and without stopping hydration, named hereafter b) and b') methodologies, respectively.

2.2. Analytical techniques

2.2.1. Scanning Electron Microscopy (SEM).

The as-prepared powder was characterized through scanning electron microscopy (SEM) (Jeol JSM-6490LV). Semi-quantitative values of Si/Al, Si/Ca and Al/Ca weight ratios were obtained by SEM combined with energy dispersive spectroscopy (EDS) by analyzing 90 different particles. The sample was previously gold sputtered.

2.2.2. Synchrotron X-Ray Powder Diffraction (SXRPD).

The SXRPD pattern for stratlingite was recorded in Debye-Scherrer (transmission) mode using the X-ray powder diffraction station of ALBA, the Spanish Synchrotron Radiation Facility

(Barcelona, Spain) (Fauth, 2013). The wavelength, 0.6202(2) Å, was selected with a double-crystal Si (111) monochromator and determined from a Si640d NIST standard (a=5.43123 Å) pattern. The diffractometer is equipped with a multy-crystal analyzer detector system especially suited for high-resolution experiments. The capillary was rotated during data collection to improve diffracting particle statistics. The data acquisition time was ~6 hours to attain very good signal-to-noise ratio over the angular range 1-45º (2θ). The temperature inside the experimental hutch was 26 ± 1ºC.

The SXRPD pattern of stratlingite was analyzed by the Rietveld method as implemented in the GSAS software package (Larson and Von Dreele, 2000). The refined overall parameters were cell parameters, zero-shift error, peak shape parameters, and phase scales. Peak shapes were fitted by using the pseudo-Voigt function (Thompson et al., 1987)

2.2.3. Laboratory X-Ray Powder Diffraction (LXRPD).

LXRPD studies were performed in reflection mode (θ/2θ) on cured BCSA cement pastes. Patterns were recorded on an X'Pert MPD PRO diffractometer (PANalytical) using strictly monochromatic CuKα1 radiation (λ=1.54059Å) [Ge(111) primary monochromator]. The X-ray tube worked at 45 kV and 40 mA. The optics configuration was a fixed divergence slit (1/2º), a fixed incident antiscatter slit (1º), a fixed diffracted anti-scatter slit (1/2º) and X'Celerator RTMS (Real Time Multiple Strip) detector, working in scanning mode with maximum active length. Data were collected from 5º to 70º (2θ) during ~2 hours. The samples were rotated during data collection at 16 rpm in order to enhance particle statistics.

2.2.4. Thermal analysis.

Differential thermal (DTA) and thermogravimetric (TGA) analyses were performed to the stratlingite powder in a SDT-Q600 analyzer from TA instruments (New Castle, DE). The temperature was varied from room temperature (RT) to 1000°C at a heating rate of 5 ºC/min. Measurements were carried out in an open platinum crucible under nitrogen flow. The weighed loss from RT to ~550ºC was assumed to be water (free and chemically bound water) and that from ~550ºC to 1000ºC was considered as CO_2.

2.2.5. Nuclear Magnetic Resonance (NMR) experiments.

^{1}H, ^{29}Si and ^{27}Al magic-angle spinning (MAS), ^{29}Si {1H} and 27Al {1H} cross-polarization (CP-MAS) experiments were conducted on a Bruker Avance-400 NMR spectrometer with a 9.39 T widebore superconducting magnet. MAS-NMR and CP-MAS spectra were recorded at room temperature (RT) with 4 mm zirconia (PSZ) rotors at a spinning rate of 10 kHz. ^{29}Si MAS NMR spectra were recorded at 79.49 MHz. Spectra were obtained after irradiating the samples with a π/2 (6 μs) pulse, relaxation delay (D1) of 30 s and 800 scans. Kaolin (δ= -91.5 ppm) respect to TMS (δ=0) was used as the external standard. ^{27}Al MAS-NMR were recorded at 104.26 MHz, with a pulse width of 2 μs, relaxation delay (D1) of 10 s and 64 scans. Chemical shifts for aluminum components were referred to an aqueous solution of $AlCl_3 \cdot 6H_2O$ (δ=0) (1 M). ^{1}H MAS-NMR spectra were recorded at 400.13 MHz. These spectra were obtained with a π/2 (5 μs) pulse, relaxation delay (D1) of 5 s and 240 scans. ^{29}Si CP MAS-NMR data were recorded on selected samples at short contact time (P15) of 1 ms and 1200 scans. In cross-polarization experiments, ^{29}Si spin gathers higher polarization from the proton-spin reservoir, favoring detection of silicon nuclei that are submitted to dipolar interactions with protons. ^{27}Al CP MAS-NMR data were recorded at contact time (P15) of 1 ms and 400 scans. In these experiments detection of Al cations located near protons will be again favored.

3. Results and discussion

3.1. Stratlingite phase sample

After several attempts to prepare crystalline stratlingite, the synthesis described in the experimental section gave the best sample. We consider the 'best' sample that containing the highest amount of stratlingite with relatively sharp powder diffraction peaks. In fact, the Rietveld Quantitative Phase Analysis (RQPA) of the SXRPD pattern gave 85.2(1) wt% of stratlingite, 9.5(1) wt% of calcite-$CaCO_3$ (ICSD-80869), 4.2(2) wt% of Vaterite-$CaCO_3$ (ICSD-15879), 0.7(1) wt% of monocarbo-AFm (ICSD-59327), and 0.4(1) wt% of plazolite (ICSD-31250). Furthermore, DTA-TGA experiments showed a weight loss of ~30 wt% between room temperature and ~550ºC. This mass loss agrees quite well with the expected mass loss for 8 molecules of H_2O of the stratlingite content, in agreement with the literature (Kwan et al., 1995; Rinaldi et al., 1990).

3.2. Stratlingite structure and microstructure

Figure 1 shows a SEM micrograph of the as-prepared stratlingite powder. It is formed by laminar particles with an average size of 1-2 μm (width) and less than 0.1 μm (thickness). Table 1 shows the obtained results by SEM-EDS, and those shown in the literature (Rinaldi et al., 1990) for the sake of comparison. These results match pretty well, although the sample studied here is slightly richer in silicon and poorer in aluminum.

The crystal structure of the bulk powder of stratlingite was studied using as starting model the structural description reported by Rinaldi et al. (ICSD-69413) from a mineral (Rinaldi et al., 1990). It must be highlighted that the anisotropic peak broadening of this sample was severe, in agreement with the SEM study, and this has to be properly modeled. For the stratlingite peak shape, the isotropic Gaussian contribution, GW, was

negligible and a Lorentzian function was used (Thompson et al., 1987). The final refined parameters were LX=0.008(1)º, LY=0.26(1)º and PTEC=0.071(1)º. The last parameter defines the anisotropic broadening along the c-axis. The anisotropic peak broadening was very strong and it can be visualized by the Full Width at the Half Maximum (FWHM) values. The (003) reflection at 2.80º (2θ) [or 12.579 Å] was quite broad with a FWHM value of 0.089º (2θ). In addition, the (110) reflection at 12.35º (2θ) [or 2.877 Å] was very sharp with a FWHM value of 0.037º (2θ). Figure 2 shows the Rietveld plot of the SXRPD pattern with the optimized structure and microstructure models. The refined unit cell parameters were a=b=5.7535(2) Å and c= 37.731(3) Å. The structural refinement includes atomic positions and isotropic atomic displacement parameters (ADPs). However, the high degree of disorder and the lack of diffraction peaks over 35º (2θ; λ=0.62Å) yields physically unrealistic iso-ADPs if no constraints were used. Therefore, all oxygen-OH, oxygen-oxo and oxygen-water were constraint to have the same value. The final Rietveld disagreement factors were R_{WP}=6.3 % and R_F=7.5 %. Table 2 shows the final refined values of the positional parameters and ADP factors.

Table 1. Si/Al, Si/Ca and Al/Ca weight ratios of the laboratory synthesized stratlingite obtained by SEM-EDS and those reported in literature.

	Si/Al	Si/Ca	Al/Ca
This study	0.7(1)	0.43(6)	0.60(8)
Literature (*Rinaldi et al.)*	0.58	0.41	0.70

Figure 3a depicts the crystal structure of stratlingite where selected atoms are labeled. Octahedral and double-tetrahedral layers are shown in detail in figures 3b and 3c, respectively, along a- and b- axes. The octahedral layer has the $[Ca_2Al(OH)_6(H_2O)_2]^+$ composition and the tetrahedral double-layer can be described as $[Si_{1.24}Al_{0.76}\square_2O_2(OH)_{4.242}(H_2O)_{0.25}]^-$ where Si/Al ratio is consistent with SEM results given in Table 1. Consequently, the tetrahedral layer may contain 2 mols of oxygen-oxo and 4.242 mols of hydroxyl groups (OH), for neutral charge of the compound, which some of them will be either μ-oxo or μ-hydroxy bridges, and the rest will be end-members.

The CIF file is also deposited. It has to be noted that the Si/Al occupancy is not possible to be deduced by X-ray diffraction because they have (almost) the same number of electrons. The occupancy factors (o.f.) for oxygen-OH (OH1 and OH2) and oxygen-oxo (O1) cannot be deduced because these sites can be partially occupied by both types of species.

Table 2.- Final position, occupation factor and ADPs from stratlingite crystal structure refinement.

Atom	type	o.f.	x	y	z	isotropic-ADP/ Å2
Al	3a	1.0	0.0000(-)	0.0000(-)	0.0000(-)	0.015(3)
Ca	6c	1.0	0.3333(-)	0.6667(-)	0.0146(1)	0.002(2)
OH1	18h	1.0	0.8311(6)	0.1689(6)	0.1046(2)	0.039(2)
OH2	36i	0.5	0.737(1)	0.043(1)	0.0273(2)	0.039(2)
O1	6c	1.0	0.6667(-)	0.3333(-)	0.1678(4)	0.039(2)
SiT1	6c	0.5	0.0000(-)	0.0000(-)	0.1212(4)	0.025(4)
SiT2	6c	0.5	0.6667(-)	0.3333(-)	0.1241(4)	0.031(4)
Ow1	3b	0.25	0.3333(-)	0.6667(-)	0.1667(-)	0.039(2)
Ow2	6c	1.0	0.3333(-)	0.6667(-)	0.0873(3)	0.039(2)

^{29}Si, ^{27}Al and ^{1}H NMR (MAS and CP-MAS) spectra for as-prepared stratlingite powders are shown in Figures 4a, 4b and 4c, respectively. The band located close to ~-86 ppm in all ^{29}Si spectra (figure 4a) could be ascribed to $Q_3(2Al)$ or $Q_2(1Al)$. However, according to the chemical formula and data from literature (Kwan et al., 1995) should be better ascribed to Q_2, because of the existence of vacancies in the double tetrahedral silicate ring structure. The double tetrahedral layer, $[Si_2Al_2O_4(OH)_8]^{2-}$, has to show a large amount of vacancies to give the formula $[Si_{1.24}Al_{0.76}\square_2O_2(OH)_{4.242}(H_2O)_{0.25}]^-$, which also explains the low tetrahedral condensation observed in ^{29}Si spectra. ^{29}Si MAS NMR also shows two small bands located at -82 and -91 ppm, assigned to $Q_2(2Al)$ and $Q_3(2Al)$, respectively. The absence of these bands in CP-MAS spectra may be related with the lower condensation (less OH groups). Hence, Q_2 is the most probable structure, which may well be assigned to open chains (Q_1 and Q_2) or to closed six-membered rings (Q_2). However, the existence of square-rings may justify the presence of an ordered alternation of Si-Al-Si-Al within them. This fact would justify the assignation of the signal at -82 ppm to $Q_2(2Al)$. Kwan et al. (1995) also observed a band at ~-90 ppm in the ^{29}Si CP-MAS-NMR spectra of stratlingite without extra alkali. This is attributed to complex Q_2 silicate species within ring structures. On the other hand, $Q_2(2Al)$, $Q_2(1Al)$ chains may exist between AFm consecutive layers. The condensation of parallel chains, based on the condensation of Si-OH groups of consecutive chains, may favor the formation of rings with four elements (Si-Al-Si-Al associations in $Q_2(2Al)$ areas).

^{27}Al MAS NMR spectrum (figure 4b) shows two bands; the first one centered at ~61 ppm, ascribed to tetrahedral Al with a shoulder at ~68 ppm related with lower condensed tetrahedral Al, and the second one located at 9.9 ppm, with higher intensity, which is related with the octahedral aluminum. Relative amounts of octa- and tetrahedral aluminum agree with the formula deduced by SEM-EDS analysis. Additionally, ^{1}H NMR spectrum shows two bands, figure 4c, one ascribed to water (5 ppm) and another one (at 2 ppm) assigned to Al-OH or Si-OH groups.

Finally, in this model, Si substituted by Al tetrahedral layers cannot exist without any cation compensating charge. Because of that, links between the two types of layers should exist, i.e. Al_{tet}-O-Ca and Al_{tet}-O-Al_{oct}. The existence of these links would justify the union between adjacent octahedral and tetrahedral layers, and would explain the lack of ^{1}H-^{27}Al polarization transference in CP-MAS experiments (absence of some peaks in ^{27}Al CP-MAS spectra). In this model, the detected partial occupations in the tetrahedral layers should not be considered as defects but as unfinished tetrahedral layers. This would justify the existence of interactions between well-defined adjacent layers, and the existence of stratlingite with different spectra.

3.3. Stratlingite in cement pastes.

Figure 5 shows raw LXRPD patterns of BCSA pastes prepared following a), b) and b') methodologies, detailed in the experimental section. These samples contain, as main phases, anhydrous β-belite and ettringite (AFt), a sulfate-bearing AFm type phase (AFm) and stratlingite as hydration products. The main peaks of the latter are marked with asterisk. The inset gives an enlarged angular range of the patterns, where (003) line, ~7° (2θ CuKα), and (110) line, ~31° (2θ CuKα), of stratlingite are shown in detail. Table 3 shows the FWHM values of these two lines and the unit cell parameters of stratlingite in all the BCSA paste patterns. On the one hand, the (003) line position is slightly shifted to higher angles, i.e. lower inter-laminar space and volume, when BCSA pastes are measured after stopping hydration. This is an indicator of some kind of stratlingite dry damaging (Zhang and Glasser, 2000), probably a joint effect of dehydration and disorder. This effect is obviously not observed in (110) line as it is not related to the inter-laminar space. The (003) line displacement is larger for the paste prepared by methodology a), which is related to higher dehydration effects. This phenomenon may be expected, as this paste was not stored under water and also, had a high surface in contact with air. On the other hand, pastes with higher degree of dehydration effect, i.e. methodology a), shows larger disorder between their layers, provoking an enlargement of FWHM value of (003) line, see Table 3. However, those lines, for instance (110), related to brucite-type layer are not influenced by this effect. Moreover, the formation of the sulfate-bearing AFm type phase is also affected by the curing methodology. Methodology a) results as the less favorable one as that phase almost did not crystallize in the sample. Table 4 shows refined profile parameters to fit stratlingite which is present in LXRPD patterns of BCSA pastes prepared by the three methodologies previously detailed. The stratlingite peak shape was fitted by a pseudo-Voigt function with both isotropic Gaussian, GW, and anisotropic Lorentzian, LY, STEC and PTEC contributions (Thompson et al., 1987). The two last parameters define the anisotropic broadening along the c-axis. The modeling of the microstructure of stratlingite is important to derive suitable RQPA results for pastes containing this phase. Figures 6a and 6c show Rietveld plots of BCSA pastes prepared following a) and b) methodologies, respectively, where the anisotropic broadening correction has been applied along c-axis. In addition, Figures 6b and 6d show the Rietveld fits by using an isotropic pseudo-Voigt function. The fit of (110) line shows a greater mismatch when the microstructure of stratlingite is not modeled. This effect has been especially dramatic in the case of methodology a) where the paste suffered dry damaging, Figure 6b. Moreover, Table 4 includes the weight percentages of stratlingite in all pastes obtained by RQPA modeling the microstructure and without any anisotropic contribution. It has to be noted that the three pastes have been prepared with the same cement, w/c ratio and at the same time of hydration by using different hydration methodologies. Consequently, phase assemblage should be almost identical. When the microstructure of stratlingite is not modeled, the obtained percentages of stratlingite present a great mismatch (see Table 4), being larger for the sample prepared following methodology a).

Table 3.- FWHM values for (003) and (110) lines (2θ CuKα), and cell parameters of stratlingite in all the BCSA paste patterns prepared by a) (sample holder+stopped hydration), b) (cylinder+stopped hydration) and b') (cylinder non-stopped hydration) methodologies.

Methodology	(003) line		(110) line		Cell parameters		
	2θ/°	FWHM/°	2θ/°	FWHM/°	a (Å)	c (Å)	V (Å^3)
a)	7.11(1)	0.25(4)	30.94(1)	0.20(1)	5.7704(4)	37.24(2)	1073.8(6)
b)	7.09(1)	0.22(1)	30.96(1)	0.20(1)	5.7705(5)	37.290(7)	1075.4(3)
b')	7.01(1)	0.18(1)	30.94(1)	0.20(1)	5.7681(5)	37.458(7)	1079.3(2)

4. Conclusions

Crystalline stratlingite has been prepared as bulk powder sample. Its AFm-type structure can be described as alternating

tetrahedral and octahedral layers. The octahedral layer (brucite-type) is formed by $[Ca_2Al(OH)_6(H_2O)_2]^+$ *units and the tetrahedral double-layer can be described as* $[Si_{1.24}Al_{0.76}\square_2O_2(OH)_{4.242}(H_2O)_{0.25}]^-$*. The structure and microstructure of stratlingite have been studied by synchrotron X-ray powder diffraction data. Its powder pattern displays strong anisotropic peak broadening with quite broad (00l) diffraction peaks. Conversely, the (hk0) diffraction peaks are relatively much sharper. This microstructure has been successfully modeled with the available anisotropic peak shape function available in the GSAS package. The refinement of the structure includes atomic positions and isotropic atomic displacement parameters (ADPs) with constraints in the oxygen-bearing species to yield to a physically realistic description. Acceptable values of* R_{WP} *and* R_F *values were obtained, 6.3 and 7.5 %, respectively.*

Table 4.- Refined anisotropic profile parameters to fit stratlingite and weight percentage of this phase obtained by RQPA of all the BCSA paste patterns prepared by a) (sample holder+stopped hydration), b) (cylinder+stopped hydration) and b') (cylinder non-stopped hydration) methodologies.

Methodology	Gaussian GW/°	Lorentzian LY/°	STEC*/°	PTEC*/°	Stratlingite (anisotropic peak shape) wt%	Stratlingite (isotropic peak shape) wt%
a)	0.64(7)	0.22(3)	0.34(-)	0.80(-)	31.2(5)	11.4(4)
b)	0.34(6)	0.40(3)	0.34(-)	0.20(1)	30.6(5)	22.5(3)
b')	0.33(5)	0.35(3)	0.34(-)	0.144(9)	28.0(5)	21.9(3)

**Anisotropic broadening correction parameters along c-axis*

^{29}Si MAS NMR spectra indicates that Q_2 *is the most probable structure, which may well be assigned to open chains (*Q_1 *and* Q_2*) or to closed six-membered rings (*Q_2*) for the double tetrahedral layer. ^{27}Al MAS NMR spectrum shows a band ascribed to tetrahedral Al with a shoulder related to a lower condensed tetrahedral Al, and another one with higher intensity is related with the octahedral aluminum.*

The stratlingite phase formed in cements pastes is sensitive to the hydration conditions. When BCSA pastes after stopping hydration are characterized through LXRPD, the (003) line position appears slightly shifted to higher angles (lower inter-laminar space and volume) compared with the similar paste but without stopping hydration. This is likely related to dehydration and disorder. This shift is even larger when the paste has suffered some dehydration during curing (apart from stopping hydration); in that case, stratlingite shows larger disorder between its layers, provoking an enlargement of the FWHM value of (00l) lines. Modeling the microstructure of stratlingite is important to derive suitable RQPA results in BCSA pastes containing this phase. This is especially relevant for pastes that suffered dry damaging.

Figure Captions

Fig. 1. Scanning electron micrograph of laboratory prepared stratlingite displaying the layered microstructure.

Fig. 2. SXRPD Rietveld plot for laboratory synthesized stratlingite. Inset shows an enlarged angular range where main peaks due to minor phases are labeled.

Fig. 3. a) Layered crystal structure of stratlingite. b) Enlarged view of the double-tetrahedral layer. c) Enlarged view of the octahedral layer.

Fig. 4. ^{29}Si, ^{27}Al and ^{1}H NMR (MAS and CP-MAS) spectra (a, b and c, respectively) for laboratory synthesized stratlingite powder.

Fig. 5. Raw LXRPD patterns of BCSA pastes prepared following methodologies a) sample holder+stopped hydration, b) cylinder+stopped hydration and b') cylinder non-stopped hydration methodologies. Main stratlingite peaks are marked with asterisk. The insets show an enlarged range where (003) and (110) lines are located.

Fig. 6. Rietveld plots for LXRPD patterns of BCSA pastes prepared by different methodologies, (a) and (b) with the anisotropic broadening correction to fit stratlingite phase and (c) and (d) without modeling the microstructure.

Acknowledgments

This work has been supported by Junta de Andalucía through P11-FQM-07517 research project. I. Santacruz thanks a Ramón y Cajal fellowship, RYC-2008-03523. Synchrotron experiments were performed in MSPD beamline at ALBA Synchrotron Light Facility with the collaboration of François Fauth.

References

Álvarez-Pinazo G, Santacruz I, León-Reina L *et al.* (2013) Hydration reactions and mechanical strength developments of iron-rich sulfobelite eco-cements. *Industrial & Engineering Chemistry Research* **52(47)**:16606−16614.

Álvarez-Pinazo G, Cuesta A, García-Maté M *et al.* (2012) Rietveld quantitative phase analysis of yeelimite-containing cements. *Cement and Concrete Research* **42(7)**:960-971.

Aranda MAG, De la Torre AG and León-Reina L. (2012) Rietveld quantitative phase analysis of OPC clinkers, Cement and Hydration Products *Review in Mineralogy & Geochemistry* **74**:169-209.

Balonis M and Glasser FP (2009) The density of cement phases. *Cement and Concrete Research* **39(9)**:733-739.

Cuberos AJ, De la Torre AG, Alvarez-Pinazo G *et al* (2010) Active iron-rich belite sulfoaluminate cements: clinkering and hydration. *Environmental Science & Technology* **44(17)**:6855-6862.

Cuesta A, Aranda MAG, Sanz J *et al.* (2014) Mechanism of stabilization of dicalcium silicate solid solution with aluminium. *Dalton Transactions* **43(5)**:2176-2182.

Cuesta A, De la Torre AG, Losilla ER *et al.* (2013) Structure, atomistic simulations, and phase transition of stoichiometric yeelimite. *Chemistry of Materials* **25(9)**:1680−1687.

Cuesta A, Losilla ER, Aranda MAG *et al.* (2012) Reactive belite stabilization mechanisms by boron-bearing dopants. *Cement and Concrete Research* **42(4)**:598-606.

De la Torre AG, Bruque S, Campo J *et al.* (2002) The superstructure of C3S from synchrotron and neutron powder diffraction and its role in quantitative phase analyses. *Cement and Concrete Research* **32(9)**:1347–1356.

Dilnesa BZ, Lothenbach B, Renaudin G *et al.* (2014) Synthesis and characterization of hydrogarnet $Ca_3(AlxFe1-x)_2(SiO_4)_y(OH)_{4(3-y)}$. *Cement and Concrete Research* **59**:96-111.

Fauth F, Peral I, Popescu C *et al.* (2013) The new material science powder diffraction beamline at ALBA synchrotron. *Powder Diffraction* **28(S2)**:S360-S370.

Fleischer M and Jambor J. (1977) New mineral names. *American Mineralogist* **62**:395-397.

García-Maté M, De la Torre AG, León-Reina L *et al.* (2013) Hydration studies of calcium sulfoaluminate cements blended with fly ash. *Cement and Concrete Research* **54**:12–20.

Gartner E and Li GS (2006) High belite-containing sulfoaluminous clinker, method for the production and the use thereof for preparing hydraulic binders" *World Patent Application WO2006/018569 A2*.

Gartner EM (2004) Industrially interesting approaches to "low - CO2" cements. *Cement and Concrete Research* **34(9)**:1489-1498.

Hentschel GV, Kuzel HJ (1976) Stratlingite, $2CaO{\cdot}A1_2O_3{\cdot}SiO_2{\cdot}8H_2O$, ein Neues Mineral. *Neues Jahrb Mineral Monatsh* 319-25.

Klaus SR, Neubauer J and Goetz-Neunhoeffer F (2013) Hydration kinetics of CA2 and CA-Investigations performed on a synthetic calcium aluminate cement. *Cement and Concrete Research* **43**:62–69.

Kuzel HJ (1976) Crystallographic data and thermal decomposition of synthetic gehlenite hydrate $2CaO{\times}Al_2O_3{\times}SiO_2{\times}8H_2O$", *Neues Jahrbuch fuer Mineralogie Monatshefte* **148**:319–325.

Kwan S, LaRosa J and Grutzeck MW (1995) ^{29}Si and ^{27}Al MASNMR study of stratlingite, *Journal of the American Ceramic Society* **78(7)**:1921-1926.

Larson AC and Von Dreele RB (2000) General Structure Analysis System (GSAS), *Los Alamos National Laboratory Report LAUR*, 86-748.

Marchi M and Costa U (2011) Influence of the Calcium Sulphate and w/c ratio on the hydration of calcium sulphoaluminate cement. *Proc 13th Int. Congress Chem of Cem*, Madrid, Spain .

Matschei T, Lothenbach B and Glasser FP (2007) Thermodynamic properties of Portland cement hydrates in the system $CaO–Al_2O_3–SiO_2–CaSO_4–CaCO_3–H_2O$. *Cement and Concrete Research* **37(10)**:1379–1410.

Matschei T, Lothenbach B and Glasser FP (2007) The AFm phase in Portland cement. *Cement and Concrete Research* **37(2)**:118–130.

McCaffrey R (2002) Climate Change and the Cement Industry. *Global Cement and Lime Magazine. Environmental Special Issue*.

Moon JH, Oh JE, Balonis M *et al.* (2011) Pressure induced reactions amongst calcium aluminate hydrate phases. *Cement and Concrete Research* **41(6)**:571–578.

Morin V, Gartner EM, Walenta G *et al.* (2011) Hydration of a belite-calcium sulfoaluminate-ferrite cement: AetherTM" *Proc 13th International Congress on the Chemistry of Cement*, Madrid, Spain.

Passaglia E and Turconi B (1982) Silicati ed Altri Minerali di Montalto di Castro-VT. *Riv Mineral Ital* **4**:97-110.

Rinaldi R, Sacerdoti M and Passaglia E (1990) Stratlingite: crystal Structure, cemistry, and a reexamination of its polytype vertumnite. *European Journal of Mineralogy* **2(6)**:841-849.

Álvarez-Pinazo G, Cuesta A, García-Maté *et al.* (2012) Rietveld quantitative phase analysis of yeelimite-containing cements. *Cement and Concrete Research* **42(7)**:960-971.

Sahu S, Havlica J, Tomková V *et al.* (1991) Hydration behaviour of sulphoaluminate belite cement in the presence of various calcium sulphates. *Thermochimica Acta* **175(1)**:45-52.

Taylor HFW (1997) Cement Chemistry. *Thomas Telford*, London, UK.

Thompson P, Cox DE and Hasting JB (1987) Rietveld refinement of Debye-Scherrer synchrotron X-ray data from Al_2O_3. *Journal of Applied Crystallography* **20**:79-83.

Wang J (2010) Hydration mechanism of cements based on low-CO_2 clinkers containing belite, ye'elimite and calcium alumino-ferrite. *PhD Thesis*. Lille, University of Lille.

Winnefeld F and Lothenbach B (2010) Hydration of calcium sulfoaluminate cements - Experimental findings and thermodynamic modeling. *Cement and Concrete Research* **40(8)**:1239-1247.

Zhang L and Glasser FP (2000) Critical examination of drying damage to cement pastes. *Advances in Cement Research* **12(2)**:79-88.

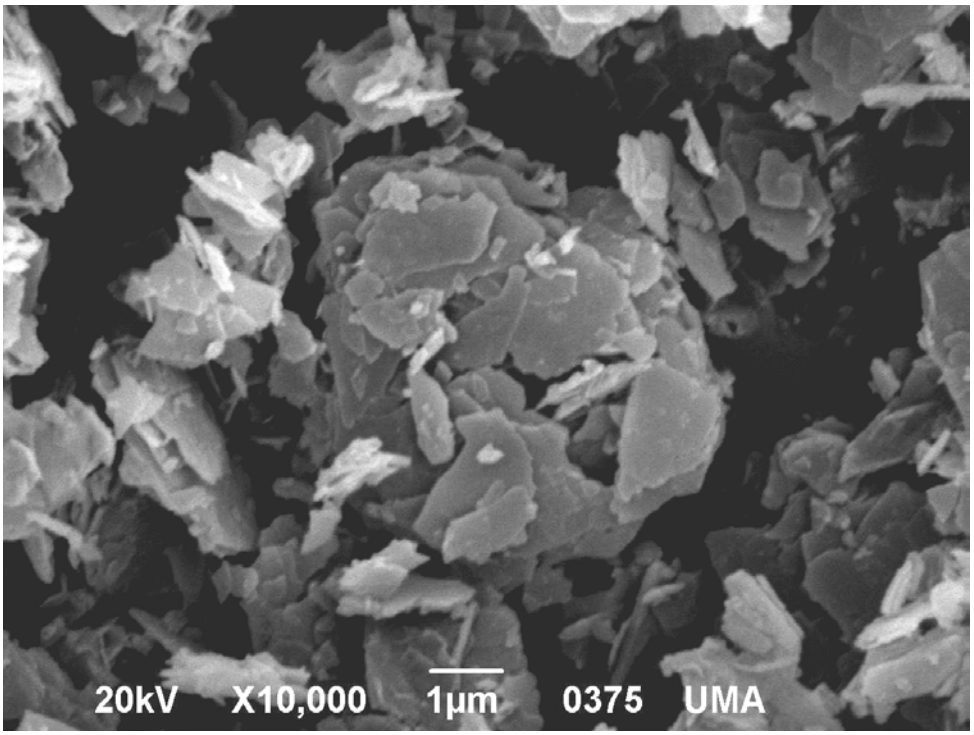

Fig. 1

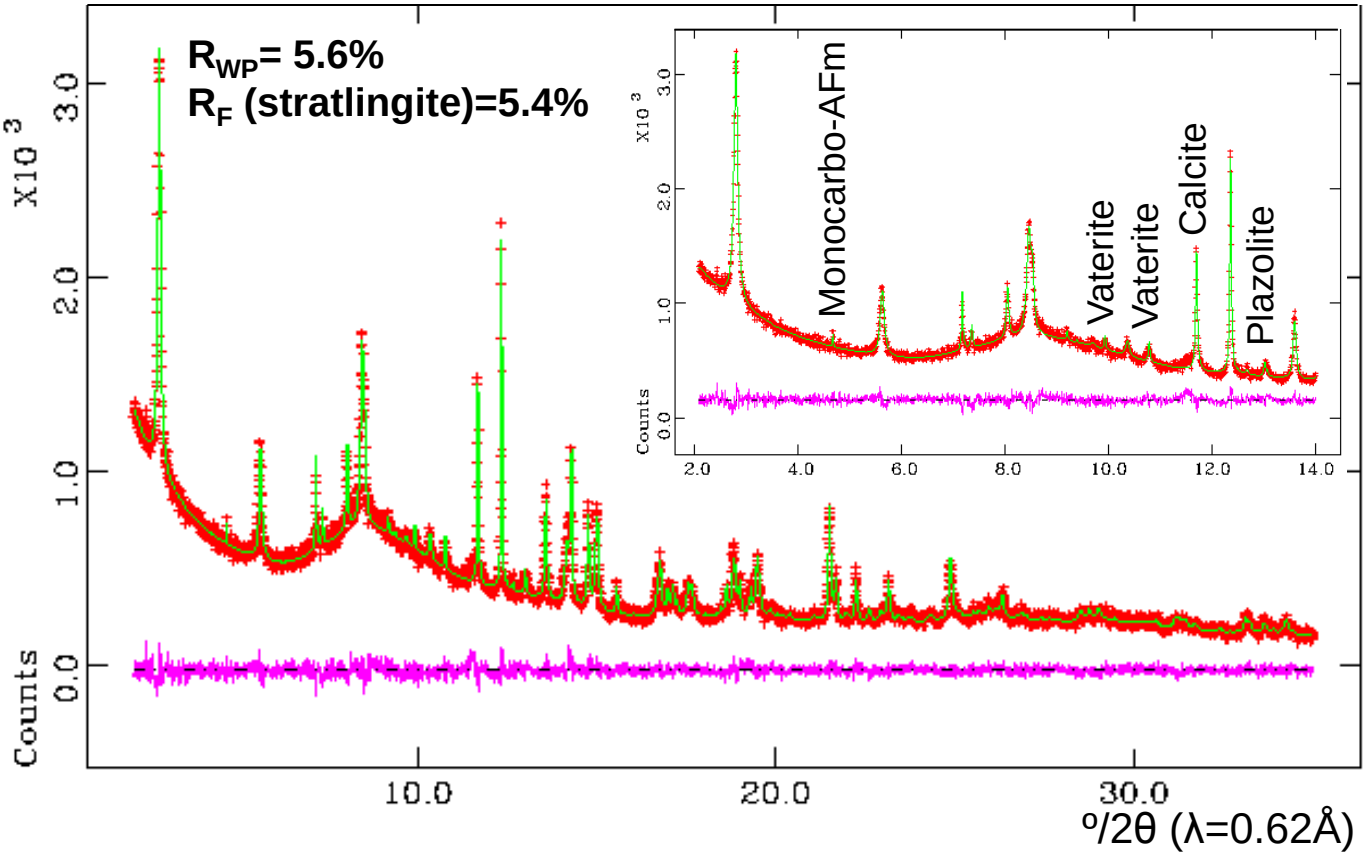
R_{WP}= 5.6%
R_F (stratlingite)=5.4%
X10 3
Counts
0.0
1.0
2.0
3.0
10.0
20.0
30.0
º/2θ (λ=0.62Å)
Monocarbo-AFm
Vaterite
Vaterite
Calcite
Plazolite
4.0
6.0
8.0
12.0
14.0

Fig. 2

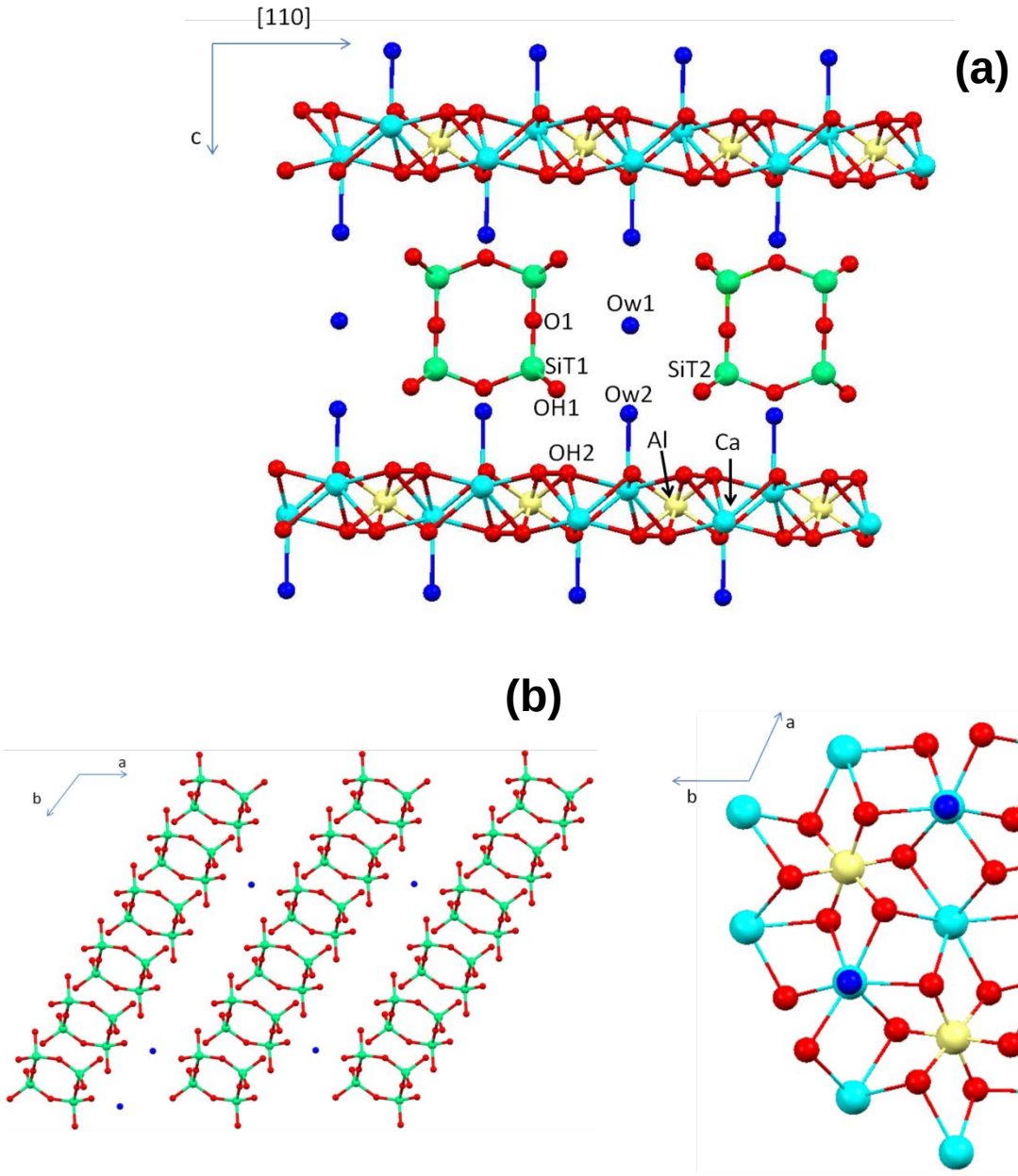

Fig. 3

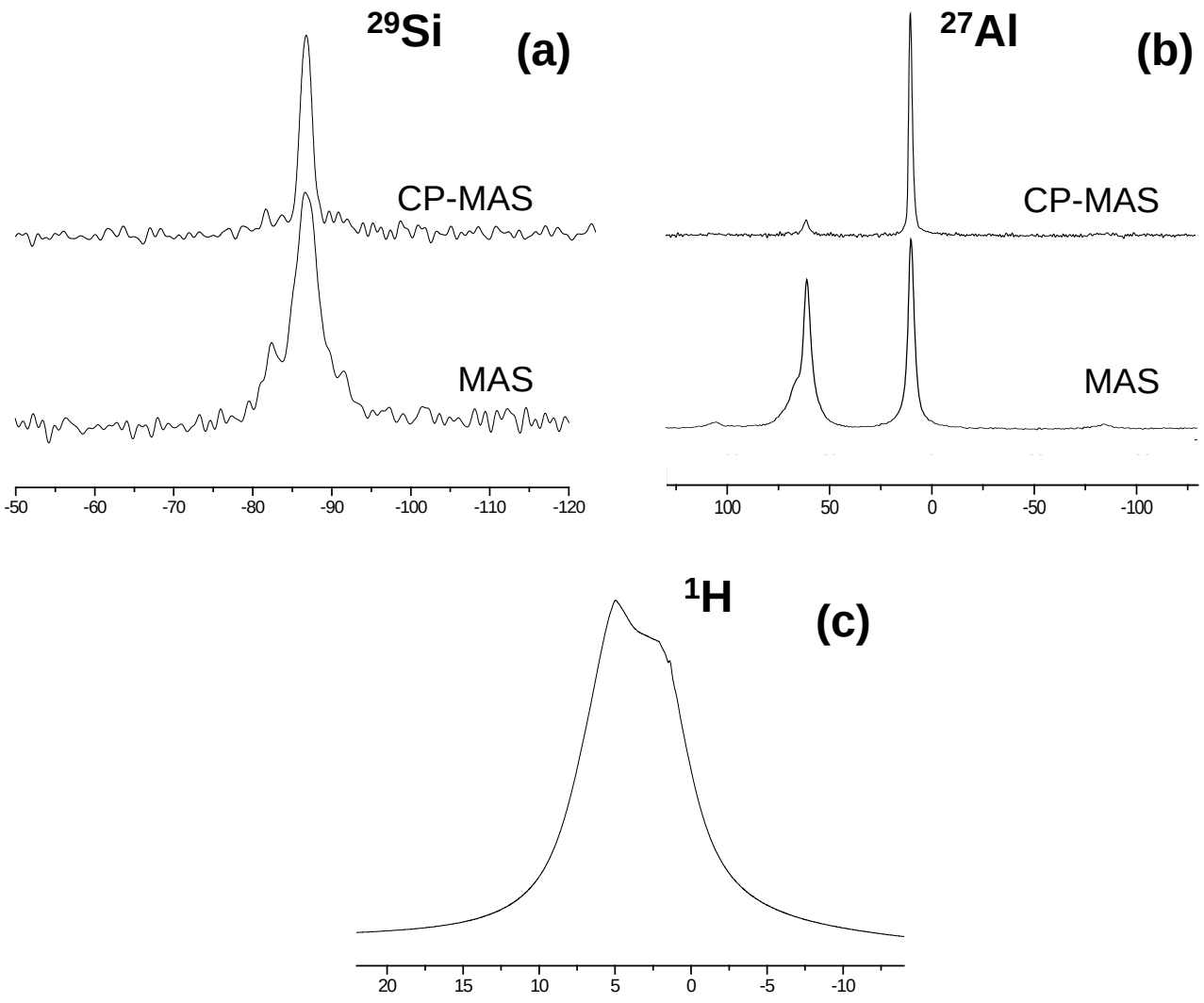
29Si
(a)
CP-MAS
MAS
-50
-60
-70
-80
-90
-100
-110
-120
27Al
(b)
CP-MAS
MAS
100
50
0
-50
-100
1H
(c)
20
15
10
5
0
-5
-10

Fig. 4

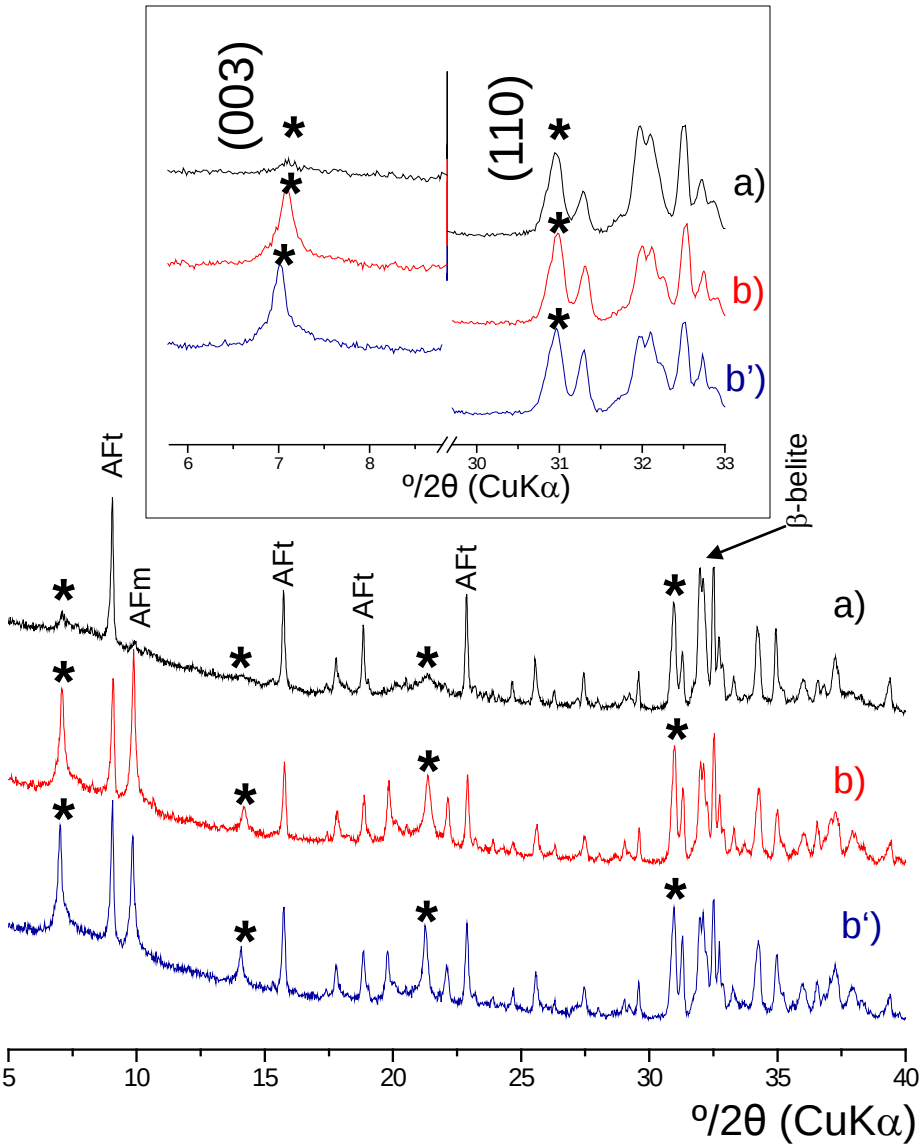
(003)
(110)
a)
b)
b')
6
7
8
30
31
32
33
º/2θ (CuKα)
AFt
AFm
AFt
AFt
AFt
β-belite
a)
b)
b')
5
10
15
20
25
30
35
40
º/2θ (CuKα)

Fig. 5

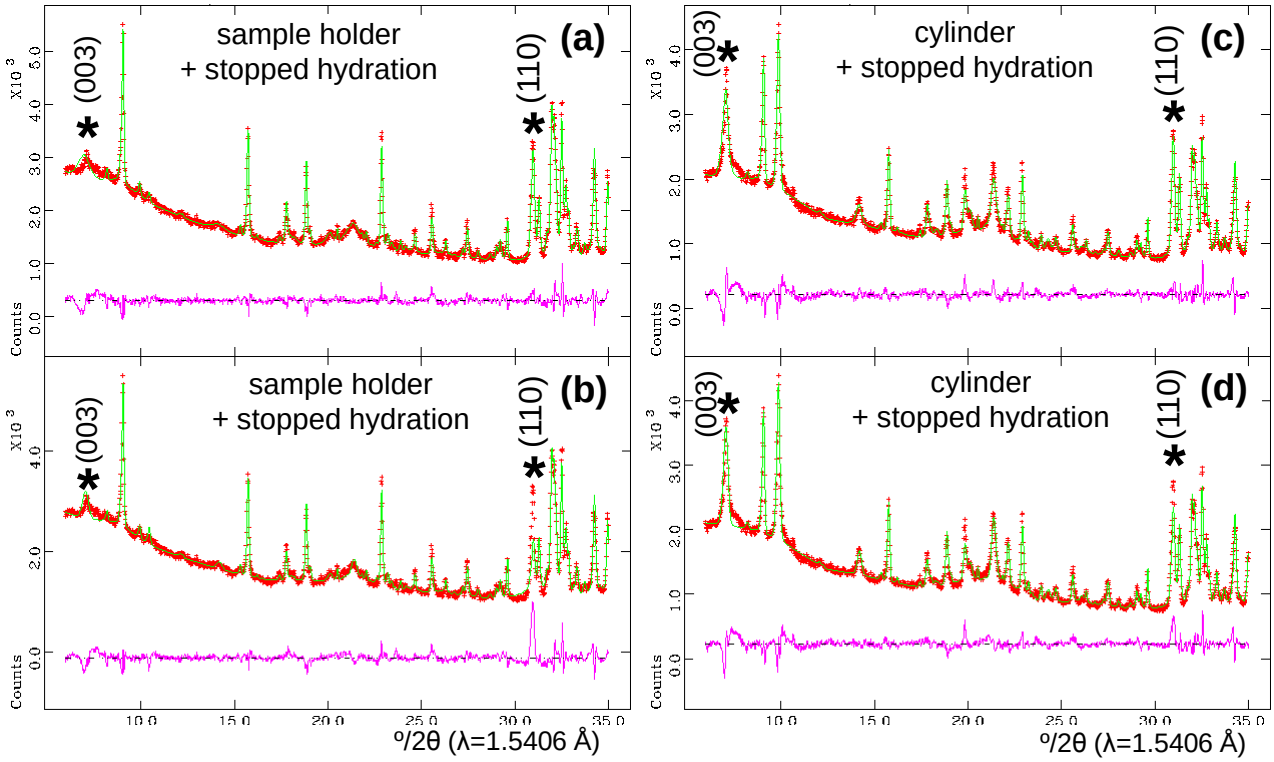
sample holder
+ stopped hydration
(a)
(003)
(110)
sample holder
+ stopped hydration
(b)
(003)
(110)
cylinder
+ stopped hydration
(c)
(003)
(110)
cylinder
+ stopped hydration
(d)
(003)
(110)
Counts
º/2θ (λ=1.5406 Å)

Fig. 6